Standing Wave Oscillations in an Electrocatalytic Reaction

Peter Strasser,* Johannes Christoph, Wen-Feng Lin, and Markus Eiswirth

Fritz-Haber-Institut der Max-Planck-Gesellschaft, Faradayweg 4-6, 14195 Berlin (Dahlem), Germany

John L. Hudson

Department of Chemical Engineering, Thornton Hall, University of Virginia, Charlottesville, Virginia 22903-2442

Received: August 26, 1999; In Final Form: November 10, 1999

Experimental standing wave oscillations of the interfacial potential across an electrode have been observed in the electrocatalytic oxidation of formic acid on a Pt ring working electrode. The instantaneous potential distribution was monitored by means of equispaced potential microprobes along the electrode. The oscillatory standing waves spontaneously arose from a homogeneous stationary state prior to a Hopf bifurcation if the reference electrode was placed close to the working electrode. Reduced electrolyte concentrations resulted in aperiodic potential patterns, while the presence of a sufficiently large ohmic resistance completely suppressed spatial inhomogeneities. The experimental findings confirm numerical predictions of a reaction−migration formalism: under the chosen geometry, a long-range negative potential coupling between distant points across the ring electrode can lead to oscillatory potential domains of distinct phase. It is further shown that the occurrence of oscillatory standing waves can be rationalized as the electrochemical equivalent of Turing's second bifurcation (wave bifurcation). In the presence of an external resistance, the coupling becomes positive throughout and leads to spatial synchronization.

1. Introduction

Ever since the early work by Joule,[1] Ostwald,[2] and Heathcote[3,4] on the electrodissolution of copper, chromium, and iron, it has been known that electrochemical processes do not necessarily proceed in a spatially homogeneous manner at the electrified interface. In recent years, research has made substantial advances in the understanding of such self-organized, nonequilibrium spatial variations of the interfacial potential and chemical concentrations near the electrochemical interface (usually referred to as "potential patterns" and "concentration patterns", respectively).[5−7]

Spatial inhomogeneities in the local reaction rate are easily observable in electrodissolution processes.[5] This is why research on spatial electrochemical patterns naturally focused first on anodic dissolution of metals such as Fe, Co, and Ni in acidic environments. In the Fe dissolution system, Hudson et al. reported spatial inhomogeneities during potentiostatic current oscillations on both disk and ring electrodes:[5,8] emerging activation and repassivation waves alternately emerged on one-half of the electrode while the other half was passive. Otterstedt et al. reported on modulated propagating pulses during Co dissolution under oscillatory conditions.[9,10] Finally, during galvanostatic potential oscillations in the Ni dissolution system, Lev et al.[11,12] observed inhomogeneous current distributions along long Ni wires. Electrocatalytic systems have only recently become the focus in the search for spatial patterns, as the spatial imaging, especially for disk electrodes, requires more sophisticated methods compared to dissolution systems.[13] While under bistable conditions transitions from one state to the other revealed accelerating,[14−16] decelerating[17,18] and even stationary catalytic reaction fronts,[19,20] experimental electrocatalysis in a spatiotemporally oscillating regime has not been reported so far.

It is generally agreed that the temporal dynamic behavior in most electrochemical systems results from the combination of nonlinear reaction kinetics and ohmic potential drop through the electrolyte.[21−23] Furthermore, theoretical and numerical work[17,24−26] indicated that spatially inhomogeneous dynamics in electrochemistry can arise through the superposition of a potential constraint provided by the potentiostat and a nonlocal migration coupling through the electrolyte. The nonlocality of the migration coupling causes local changes in the potential distribution to be felt instantaneously everywhere along the electrochemical interface with the coupling varying with distance. In fact, under certain conditions experiments evidenced a negative long-range, but positive short-range potential coupling through the electrolyte:[18,19,25] When operated under bistable conditions, this coupling function enabled remote triggering of activation fronts.[17]

The present paper reports the experimental investigation and the theoretical description of complex potential patterns across the electrode during an oscillatory electrocatalytic reaction under conditions where the controlled external potential of the working electrode is held constant (potentiostatic conditions). In particular, the dependence of the pattern formation on external parameters (chemical concentrations, geometry, and ohmic series resistance) is considered. As experimental oscillatory system, the electrocatalytic oxidation of formic acid on Pt electrodes was chosen, since its temporal dynamics is well understood.[18,23,27]

2. Experimental Section

Experimental Setup. The electrochemical three-electrode, one-compartment arrangement employed throughout all experi-

* Corresponding author. E-mail: strasser@fhi-berlin.mpg.de.

10.1021/jp993061w CCC: $19.00
Published on Web 02/12/2000

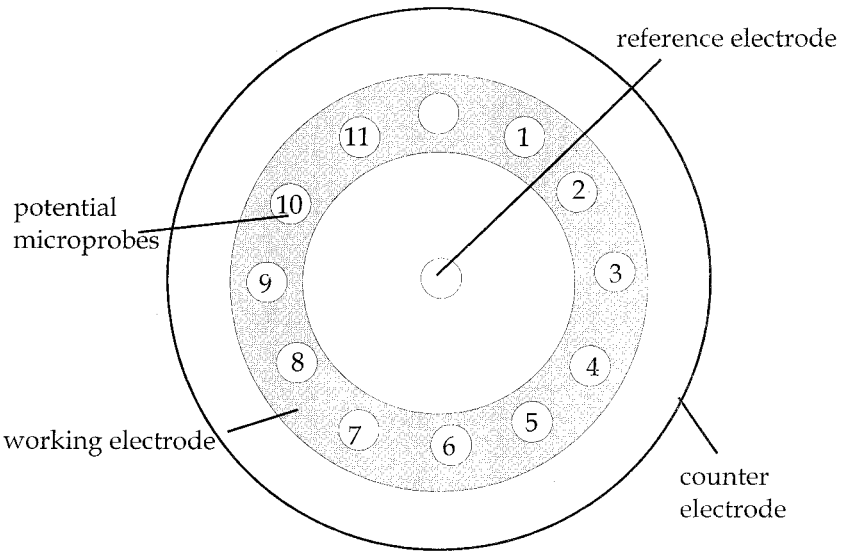

Figure 1. Schematic topview of the electrode setup. The potential microprobes (1 through 11) are separated by 30° angles. The 12 position is not monitored. The counter electrode was placed 60 mm above the plane of the other electrodes.

ments is shown in Figure 1. The working electrode (WE) consisted of a polycrystalline Pt ring electrode of 32.5 and 42.5 mm inner and outer diameter, respectively, and of 0.1 mm thickness. This corresponds to a geometrical surface of approximately 12 cm^2. A concentric Pt wire ring (1 mm wire thickness, 70 mm ring diameter, platinized for some experiments) served as counter electrode. A Luggin−Haber capillary containing a Hg/Hg_2SO_4 reference electrode was placed in the center of the working electrode: This arrangement provided a symmetrically located point within the electrolyte with a constant potential with respect to the WE.

Eleven potential microprobes were placed along the WE close to the electrode surface (100−300 μm distance) in order to measure the spatial distribution of the local electrode potential. Each microprobe consisted of a glass tube with a microcapillary (100−200 μm inner diameter), hosted a Hg/Hg_2SO_4 reference electrode, and was filled with a 0.5 M Na_2SO_4 solution (Merck, p.a.). A trigger-pulse electrode not used in the present experiments occupied the 12-position along the WE (see Figure 1) which could therefore not be monitored.

Electrode pretreatment involved chemical cleaning with concentrated H_2SO_4 (suprapure) or concentrated $KMnO_4$ solution in order to remove spurious organic compounds. Prior to experiments, voltammetric cycling between −500 mV and +600 mV was performed until a stable, reproducible cyclic voltammogram had been obtained. For spontaneous oscillations to occur without external series resistance, the WE was kept at low potentials (−400 mV) for several minutes to ensure sufficient CO poisoning of the catalytic surface, followed by a slow anodic scan (5−20 mV/s) into the oscillatory region.

Electrolyte solutions included mixtures of 0.05 M HCOONa/0.025 M H_2SO_4 as well as 0.025 M HCOONa/0.0125 M H_2SO_4 (HCOONa p.a., H_2SO_4 suprapure). The mixtures were used to leverage the buffering effect of the fomiate/formic acid system (pH ∼2.7).

A home-built potentiostat (Electronic Lab, Fritz-Haber-Institut) was used throughout. During the experiments, the instantaneous local electrode potentials were 10-fold amplified, inverted, and then sampled by a A/D multiplexer at approximately 1 kHz. The final potential signals corresponded to the local potential drop between the WE and the individual locations of the probe capillaries near the electrode and, therefore, reflected qualitatively the instantaneous local double layer potentials. The spatial potential distributions are reported as measured without any further data processing. The software for visualizing the measured data (Origin 5.0, Microcal Inc.) performed an automatic interpolation between the eleven discrete potential values.

Operating Conditions. As outlined in refs 18, 23, and 27, the formic acid oxidation on Pt under potentiostatic conditions exhibits low catalytic activity at both low and high overpotentials. At intermediate overpotentials, the electrocatalytic systems displays a kinetic bistability between an active, high-current and a passive, low current state. In addition, near the anodic edge of the active state, there is a range of overpotentials where the overall current becomes oscillatory. The following experiments refer to operating points (fixed applied outer potentials U_{ex}) inside this regime of oscillatory total catalytic reaction rate.

3 Results

3.1. Experiments. Figure 2a and b display the spatiotemporal profile of the local potential along the working ring electrode during spontaneous oscillations of the total current. Clearly visible is an inhomogeneous distribution periodic in time and space. While one-half of the working electrode exhibits strong catalytic activity indicated by a low local potential (see electrodes 7−11 at $t \sim 109$ s in Figure 2b), the other half of the catalytic interface displays strong passivation, that is, high local potentials (see electrodes 1−5 at $t \sim 109$ s in Figure 2b). Near the ring position 6, the amplitude of the temporal potential variations is significantly smaller and appears as a kind of spatial node in the overall wavelike pattern. Due to the boundary conditions, a second node-like point must lie near the ring position 12 which could not directly be monitored. Thus, the spatiotemporally oscillatory structure can be considered as far-from-equilibrium and therefore dissipative equivalent of a "standing-wave" pattern typically found in energy-conserving systems. Opposite positions along the working electrode are characterized by a 180° shift in their individual phases.

Figure 3 shows the time evolution of the total current I_{tot}, (top part), and the local current at position 6 (middle part) and position 2 and 8 (bottom part): I_{tot} exhibits a dynamical period-2 pattern consisting of two subsequent current spikes; as concluded from Figure 2, position 6 shows a reduced potential amplitude, whereas positions 2 and 8 exhibit a complex antiphase behavior

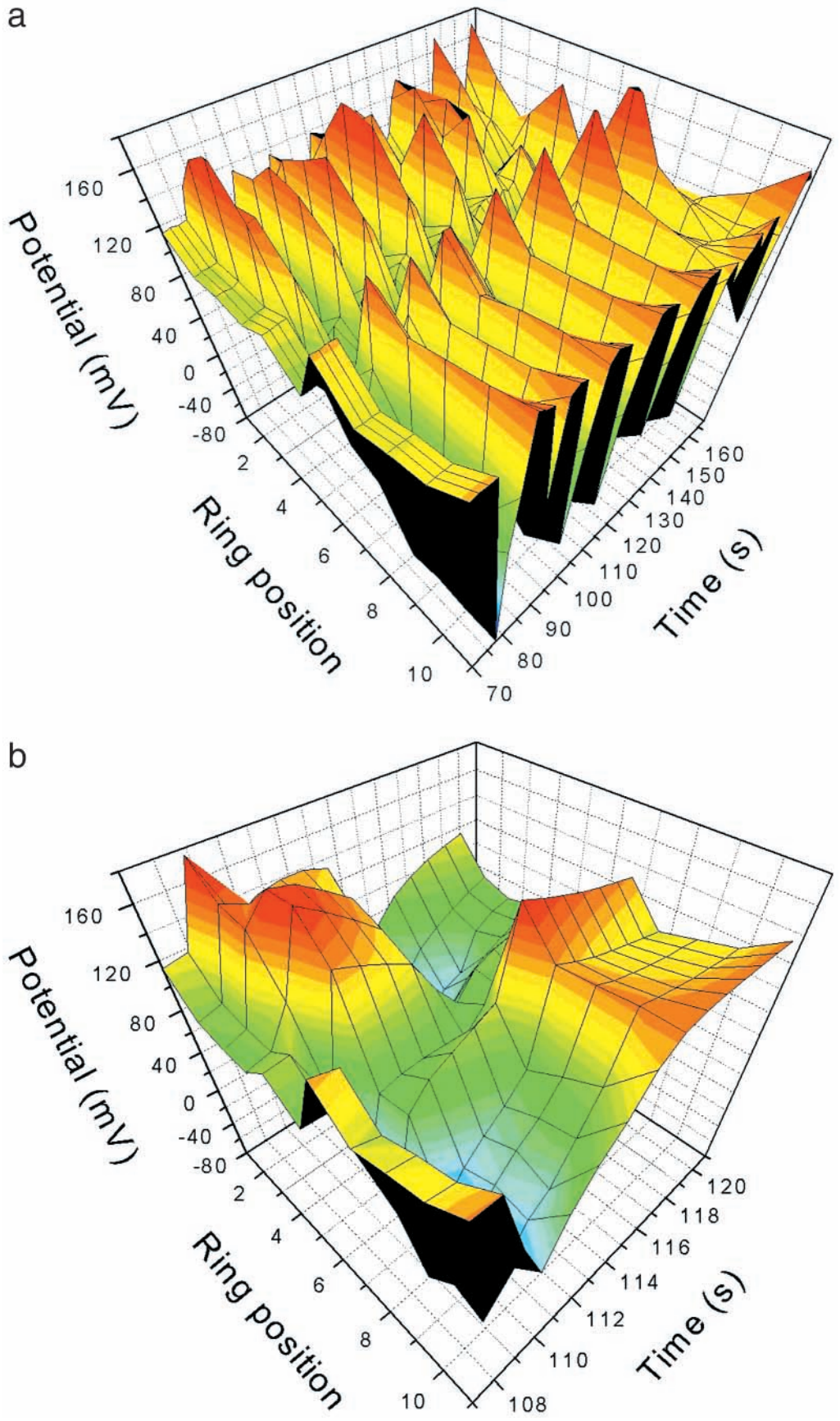

Figure 2. (a) Spatiotemporal evolution of the local potential in front of the Pt WE during formic acid oxidation under oscillatory total currents. The potential distribution displays an oscillatory standing wave pattern. $U_{ex} = 325\ mV$, 0.05 M HCOONa/0.025 M H_2SO_4, no stirring, the oscillations have been induced by a homogeneous 200 ms/+200 mV potential pulse applied to the WE. (b) Blowup of one spatiotemporal period given in a.

with large amplitudes. In Figure 3 a slow drift of the system dynamics is discernible by the changes in the oscillatory wave forms of the individual local potentials. The drift is presumably due to changes in the surface conditions associated with

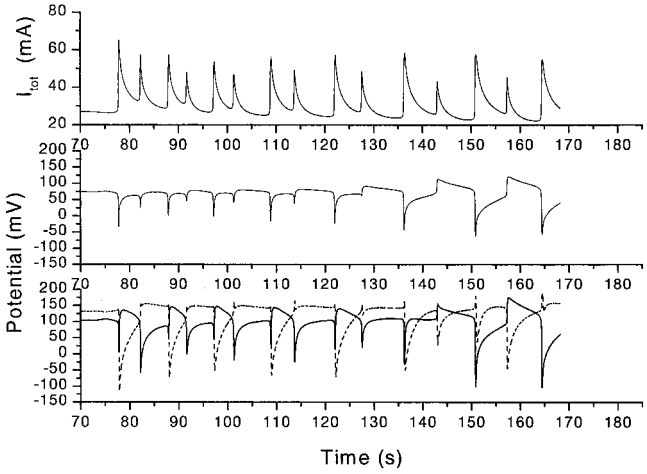

Figure 3. Local time series of the total current (top part), the local potentials at positions 6 (middle panel), and at position 2 and 8 (bottom part) during the measurement in Figure 2.

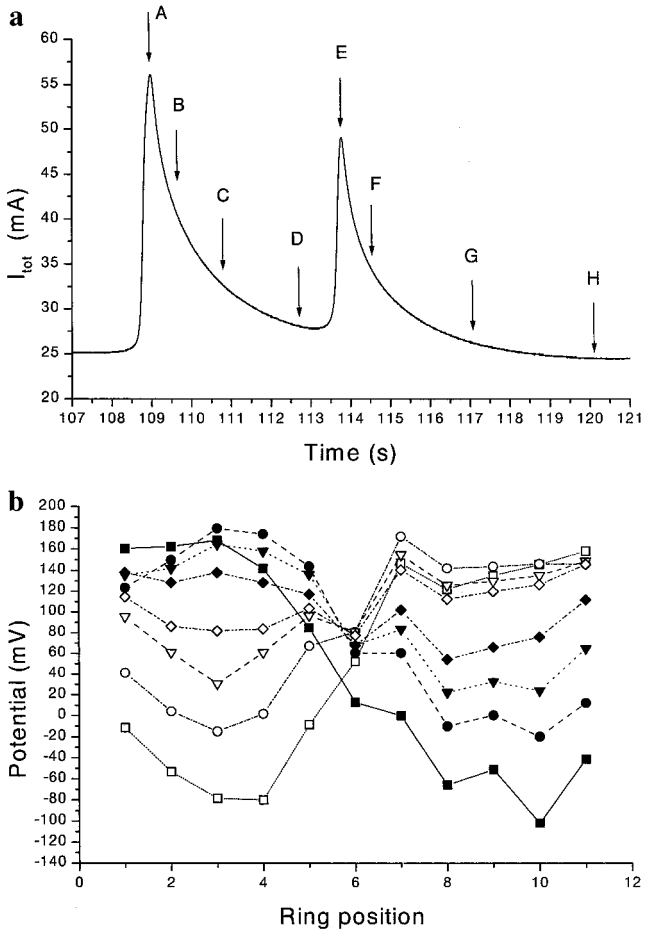

Figure 4. (a) Blowup of a period-2 cycle in I_{tot} from Figure 3. The letters indicate 8 time instances for which the spatial profiles are given in b. (b) Spatial potential profiles at subsequent time instances corresponding to a. A (filled squares), B (filed circles), C (filled triangles), D (filled diamonds), E (open diamonds), F (open triangles), G (open circles), and H (open squares).

sustained rate oscillations. Figure 4a and b point out various instantaneous spatial potential profiles during one period of I_{tot}. The letters A through H in Figure 4a indicate the instantaneous value of I_{tot}, while Figure 4b displays the corresponding spatial potential distribution: Large total currents are related to pronounced spatial inhomogeneities along the working electrode (A,E). In contrast, nearly homogeneous potential profiles result

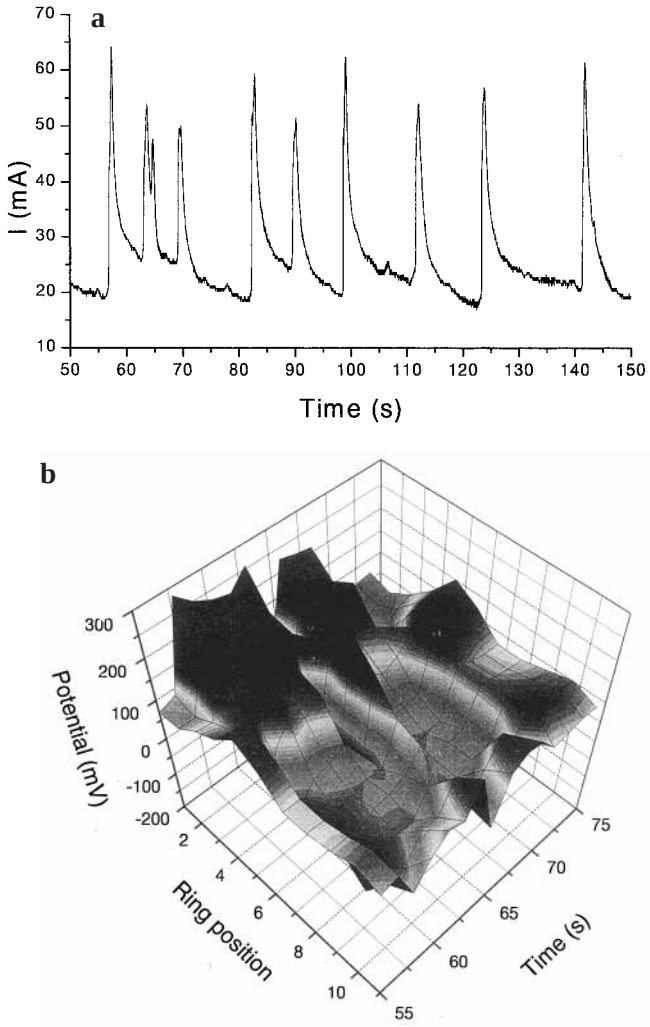

Figure 5. (a) Aperiodic time-series of the total current I_{tot} during formic acid oxidation at low electrolyte concentrations. U_{ex} = 282 mV, 0.025 M HCOONa/0.0125 M H_2SO_4, no stirring. (b) Spatiotemporally turbulent local potential distribution near the WE corresponding to the current profile given in a.

in a comparatively low catalytic activity (D,H). The latter finding apparently stems from the comparatively low activity of the node near position 6.

At lower electrolyte concentrations and different values of the outer potential, complex aperiodic spatiotemporal behavior was observed. Figure 5a displays the aperiodic time-evolution of I_{tot} with the corresponding space-time dynamics of the local potential given in Figure 5b. Interestingly, even in the aperiodic regime one can still discern an antiphase behavior between opposite points along the working electrode. So far, all experiments have been performed without an external resistance. When adding an ohmic resistance R_{ex} in series to the electrochemical cell ($R_{ex} > 4\Omega$), the spatiotemporal potential profile became immediately synchronized in space. A typical resulting time series is given in Figure 6. Complete synchronization was observed irrespective of the value of the outer applied potential within the oscillatory range or the electrolyte concentrations. Once synchronized, the time-variations of the local potential directly reflected the instantaneous total current I_{tot}.

3.2. Model Calculations. Reference 25 presented a general integral formalism for the description of the dynamics of electrochemical reaction−migration systems based on general principles of electrodynamics. The formalism was considered in detail for a geometry comparable to that employed here, that

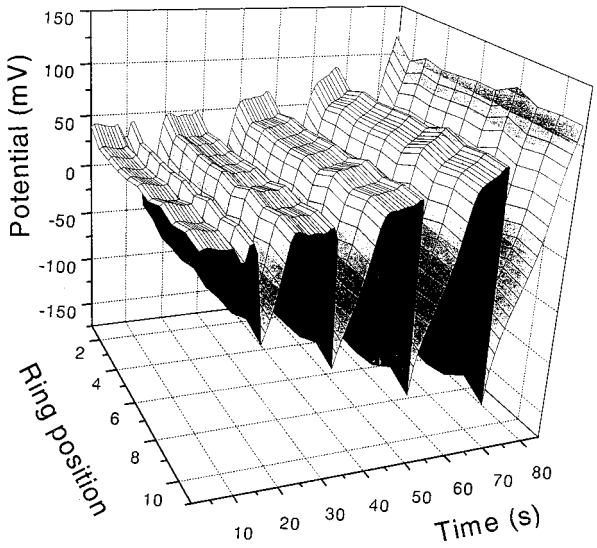

Figure 6. Synchronized local potential distribution during oscillatory formic acid oxidation in the presence of an external resistance $R = 10\Omega$. $U_{ex} = 396$ *mV*, 0.1 M HCOONa/0.05 M H_2SO_4, no stirring.

is, the WE was assumed to be a thin annulus of outer radius 1 and inner radius $A = 0.9$ embedded in an insulator with a pointlike RE located in its center, while the CE was located at infinite distance. To model oscillatory spatiotemporal patterns along the ring position x along the WE under potentiostatic conditions, the evolution equation for the local interfacial potential $\phi(x,t)$

$$C_{dl}\,\dot{\phi}(x,t) = -i_{reac}(\phi,c) + \frac{U_{ex} - \phi}{\rho_{tot}} + \kappa\int_0^1 H_B(|x - x'|)[\phi(x',t) - \phi(x,t)]\,dx' \quad (1)$$

was combined with an equation for the slow dynamics of a chemical variable $c(x,t)$ with time scale ϵ

$$\dot{c}(x,t) = \epsilon[-i_{reac}(\phi,c) + 1 - c] \qquad \text{where} \qquad i_{reac}(\phi,c) = ck(\phi) \quad (2)$$

Here, C_{dl} denotes the double layer capacity, i_{reac} the local faradaic current density, $k(\phi(x,t))$ the faradaic reaction rate, U_{ex} the outer applied potential, ρ_{tot} the total resistance, and κ the conductivity of the electrolyte. At the heart of the spatial integral coupling lies the spatial coupling function $H_B(|x - x'|)$ which represent the coupling between two points x and x' along the WE. Due to the symmetry of the electrode geometry, H_B is simply a function of the distance $|x - x'|$ of two points. The functional form of H_B is strongly determined by a space independent parameter B according to

$$H_B(|x - x'|) = H_0(|x - x'|) + \frac{h^2 B}{1 + hB} \text{ with } h = -\int_0^1 H_0(|x - x'|)\,dx' \quad (3)$$

Here, $H_0(|x - x'|)$ denotes the coupling function at $B = 0$ (see Figure 7a middle curve). The parameter B depends on the external series resistance R_{ex}, on the aspect ratio of WE and RE, β, that is, the distance between RE and WE normalized to the diameter of the WE, and on the inner diameter of the annulus A:[25]

$$B = R_{ex}\,\pi\kappa(1 - A^2) - \sqrt{1 + \beta^2} + \sqrt{A^2 + \beta^2} \quad (4)$$

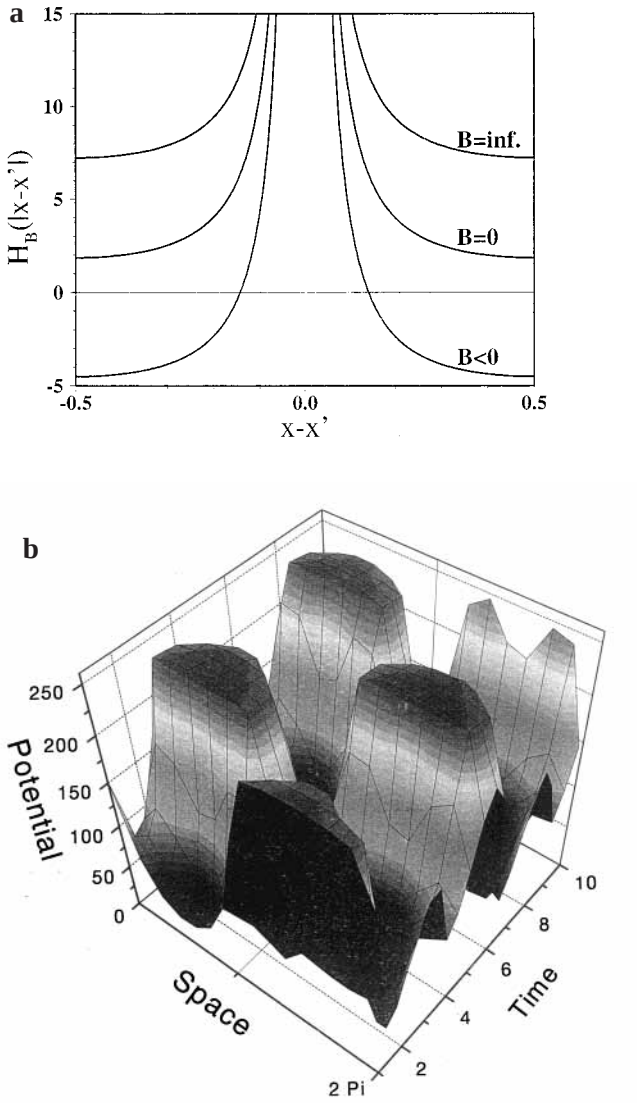

Figure 7. (a) Coupling function H_B for different values of the parameter B; H_B represents the coupling between two points x and x' along the interface with distance $x - x'$. (b) Calculated oscillating standing wave of the interfacial potential in the two-variable reaction-migration model (eqs 1 and 2) past a Wave bifurcation. parameters and functions: $k(\phi(x,t)) = \sum_{i=1}^{3} a_i\phi^i(x,t)$ with $a_1 = 0.55932$, $a_2 = -4.725 \times 10^{-3}$, $a_3 = 10^{-5}$; $U_{ex} = 239$, $\rho_{tot} = 125$, $\epsilon = 10^{-4}$, $\kappa = 7.04 \times 10^{-4}$, $C_{dl} = 1$, $A = 0.9$, $R_{ex} = 0$, $\beta = 0$.[25]

Figure 7a displays the function H_B for three different values of the parameter B. The absence of an external series resistance in combination with a large distance between WE and RE results in B $\lesssim$ O and H_B takes on the shape of the middle curve in Figure 7a. For sufficiently small distances between WE and RE, B takes on large negative values shifting H_B by a space-independent negative offset. For sufficiently negative B, the coupling function may become negative for large $|x - x'|$ as seen in the bottom curve in Figure 7a. In the presence of an external ohmic resistance, B increases and gives rise to a positive offset of H_B. For sufficiently large ohmic resistances, the negative offset caused by the geometry is overcompensated by the positive offset of the resistance and both neighboring and remote points along the WE experience a strong positive and therefore synchronizing coupling (top curve in Figure 7a). For parameters given in the caption, Figure 7b presents the numerical spatiotemporal dynamics of eq 1 and 2. The numerical solution exhibits an oscillatory standing wave born in Turing's second bifurcation[28] (wave bifurcation[29]) on the stable stationary side

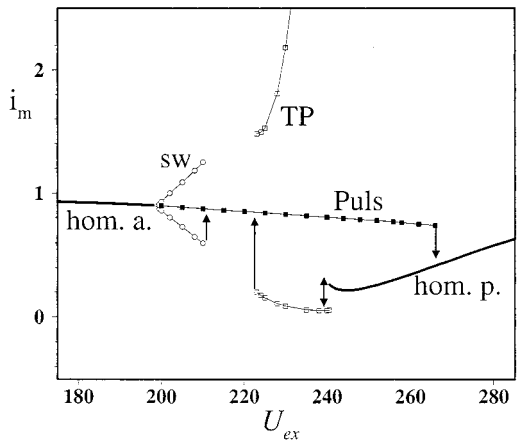

Figure 8. One-parameter bifurcation diagram of model eqs 1 and 2 at $\rho_{tot} = 40$. The maxima and minima of the total current density i_m of the occurring patterns are plotted against the outer applied potential. sw oscilatory standing waves, hom.a. = homogeneous active stationary state, TP target patterns, Puls = pulse solution branch, hom.p. = homogeneous passive stationary state. All other parameters as in Figure 7b.

of a local Hopf bifurcation. In accordance with experiments, the calculation assumed the RE in the plane of the WE ($\beta = 0$) in the absence of an external resistance R_{ex} leading to $B = -0.1$. The faradaic reaction rate $k(\phi(x,t))$ was chosen to be N-shaped[25] making the model belong to the generic mechanistic class of NDR oscillators (NDR: negative differential resistance).[6,7,18,30]

The one-parameter bifurcation diagram in Figure 8 illustrates the dominating dynamical patterns found in the theoretical model. The maxima and minima of the total current density i_m of the respective patterns are plotted against the outer applied potential U_{ex} at constant total resistance ρ_{tot}. Oscillatory standing wave solutions (sw) branch off from a homogeneous active stationary solution (hom.a.) in a wave bifurcation at $U_{ex} \sim 200$. Increasing U_{ex}, the sw solutions become transient and transform into travelling pulses for long integration times (arrow to pulse solutions). Past the first local Hopf bifurcation ($U_{ex} \sim 217$) the bifurcation diagram indicates a bistability between target patterns (TP)[25,29] and pulses, while past the second local Hopf bifurcation ($U_{ex} \sim 241$), pulse solutions coexist with a homogeneous passive stationary state (hom.p.).

For sufficiently large external resistances R_{ex}, B became positive and the numerical solutions of the model exhibited spatially homogeneous regimes throughout.

4. Discussion

The experimental results have demonstrated the self-organized occurrence of sustained spatiotemporal inhomogeneities in the interfacial potential and, consequently, in the electrocatalytic activity along a ring WE under potentiostatic conditions. The observed dynamical states with broken spatial symmetry involved oscillatory standing waves and irregular patterns; these regimes occurred at overpotentials with oscillatory total currents if the reference electrode was sufficiently close to the WE. To the best of our knowledge, this is the first report on electrochemistry with a transition from a stationary state to an oscillatory standing wave. In addition, the use of an ohmic resistance has presented an easy and reproducible way to deliberately suppress spatial inhomogeneities and, thus, to control the dynamical spatial state of the catalytic system. The experiments confirm predictions of a recently proposed reaction-migration formalism[17,25,26] for the description of spatiotemporal patterns in electrochemistry. The formalism provided an illustrative explanation how wave instabilities as well as the resistance-induced synchronization arise in electrochemical systems: the nonlocal migration coupling across the electrolyte (cf. Figure 7a for $B = 0$) is superimposed by a geometry-dependent negative offset due to the action of the potentiostat; the superposition results in an instantaneous negative coupling between distant points on the electrode. In the presence of a sufficiently large ohmic resistance, however, the mutual coupling of two points becomes positive throughout and is therefore strongly synchronizing.

In his famous paper on pattern-forming mechanisms,[28] Alan Turing described two types of diffusion-induced bifurcations from a homogeneous stationary state to sustained inhomogeneous patterns in reaction−diffusion-systems (RDS): One bifurcation results in stationary standing waves and is usually referred to in the literature as the "Turing bifurcation".[31−36] A crucial prerequisite for its occurrence was the difference in the diffusivities of the activator and the inhibitor species; the diffusion constants determined the intrinsic wavelength of the evolving pattern. Experimental examples of Turing patterns include the chlorite-iodide-malonic-acid (CIMA) reaction[33,34] or the methylene blue/HS^-/O_2 oscillator during polymerization of acrylamide.[37,38] Turing's second diffusion-induced bifurcation[28] leads to oscillatory standing waves in RDS at operating points where the local dynamics remains stable, and the bifurcation was later referred to as "wave bifurcation".[29,39] The wave bifurcation requires an additional third variable the diffusion coefficient of which has to be comparatively fast and determines the intrinsic wavelength of the resulting time-dependent wave solution. Such oscillatory standing wave regimes in RDS were investigated theoretically;[29,39,40] the only experimental example to date is the CO-oxidation on Pt(110).[41,42]

First, consider the limiting case where the inhibitor dynamics is fast and its diffusivity approaches infinity. In the resulting model, the inhibitor can be eliminated adiabatically which yields a one-variable model with a negative global coupling superimposed on the local positive diffusion coupling of the activator. The negative global coupling can give rise to stationary domains which have indeed been observed in heterogeneously catalyzed reactions.[43−46] An electrochemical equivalent occurs under geometries where the coupling of remote points along an electrode becomes negative due to a negative global coupling of the potentiostat action, if the RE is close to the WE.[19,25] The negative global coupling is superimposed on the positive, nonlocal migration coupling of the interfacial potential (see Figure 7a, middle curve, $B = 0$). The superposition yields a coupling function as shown in the bottom curve, Figure 7a ($B < 0$). The resulting electrochemical Turing-like patterns take on a wavelength which is solely determined by the system length, that is, the simplest inhomogeneous mode complying with the boundary conditions prevails. Experimentally, stationary domains in an electrochemical system with negative global coupling were recently reported by Grauel et al.[19] in the reduction of $S_2O_8^{2-}$ ions on Ag electrodes.

Now, consider the limiting case where the diffusivity of the third variable of a three-variable RDS exhibiting a wave bifurcation becomes infinity. The resulting global coupling in the remaining two-variable RD model gives rise to stationary, but time-dependent domains.[47,48] In analogy to the previous paragraph, the electrochemical equivalent of the resulting two-variable models involves the interfacial potential with nonlocal migration coupling superimposed by the negative global coupling (eq 1) as well as a slow chemical variable (eq 2). Under stationary local dynamics, the reaction-migration (RM) formal-

ism exhibits the electrochemical equivalent of a wave bifurcation (Figure 2). Just as with Turing's first bifurcation, the wavelength of the time-dependent patterns is determined by the system length (see Figure 2 and Figure 7b).

To summarize, the electrochemical equivalents of both Turing bifurcations occur for negative long-range coupling, they require one variable less than in RDS (1 and 2 instead of 2 and 3), and the instabilities occur with the largest possible wavelength because of the very fast coupling.

Under oscillatory local dynamics, a variety of further inhomogeneous patterns such as target patterns or travelling pulse solutions was predicted in three-variable RD systems[28,29,39,49] and likewise in the two-variable RM formalism with negative long-range coupling (see Figure 8).[25,26] These regimes were indeed observed experimentally during the Co electrodissolution in acidic media.[25,50]

Besides their significance in the investigation and understanding of pattern formation in chemical reaction−migration systems, spatiotemporally oscillatory regimes can provide operation modes which may offer superior characteristics compared to stationary operation in terms of catalyst activity and average catalytic yield. In the oxidation of small organic compounds such as formic acid and methanol, the space-time periodic recovery of the activity of the electrode by CO removal may lead to an increased and prolonged activity of the noble metal electrode. In fact, one finds a marked current increase in the oscillatory regimes comparing the time-averaged oscillatory currents during formic acid oxidation on Pt electrodes with those of the stationary operation points at constant applied potential.[27,51,52] Moreover, in catalytic systems operated under conditions where the coupling between remote points on the catalytic interface is negative, the inherent antiphase dynamics would be expected to prevent an entire, homogeneous poisoning of the reactive electrode, since partial poisoning at some point on the electrode would enhance the catalytic activity at a remote location; thus, the electrocatalytic WE interface would rather slip into dynamical regimes such as standing waves, travelling waves or spatiotemporal turbulence. The present study therefore also intends to stimulate further studies toward the exploitation of patterned reactive states for electrocatalysis.

Acknowledgment. Helpful discussions with Katharina Krischer are gratefully acknowledged. This work was supported by the Deutsche Forschungsgemeinschaft under SFB 555.

References and Notes

(1) Joule, J. *Philos. Mag.* **1844**, *24*, 106.
(2) Ostwald, W. *Z. Phys. Chem.* **1900**, *35*, 204.
(3) Heathcote, H. *Z. Phys. Chem.* **1901**, *37*, 368.
(4) Heathcote, H. *J. Soc. Chem. Ind.* **1907**, *26*, 899.
(5) Hudson, J. L.; Tsotsis, T. T. *Chem. Eng. Sci.* **1994**, *49*, 1493.
(6) Koper, M.T. M. *Adv. Chem. Phys.* **1996**, *92*, 161.
(7) Krischer, K. Principles of temporal and spatial pattern formation in electrochemical systems. In *Modern Aspects in Electrochemistry 32*; Bockris, J. O., Conway, B, White, R. E., Eds.; Plenum Press: New York, 1999.
(8) Hudson, J.; Tabora, J.; Krischer, K.; Kevrekidis, I. *Phys. Lett. A* **1993**, *179*, 355.
(9) Otterstedt, R.; Plath, P.; Jaeger, N. I., Hudson, J. *Phys. Rev. E* **1996**, *54*, 3744.
(10) Otterstedt, R. D.; Plath, P.; Jaeger, N.; Sayer, J.; Hudson, J. *Chem. Eng. Sci.* **1996**, *51*, 1747.
(11) Lev, O.; Sheintuch, M.; Pismen, L.; Yarnitzky, C. *Nature* **1988**, *336*, 488.
(12) Lev, O.; Sheintuch, M.; Yarnitzky, H.; Pismen, L. *Chem. Eng. Sci.* **1990**, *45*, 839.
(13) Flätgen, G.; Krischer, K.; Pettinger, B.; Doblhofer, K.; Junkes, H.; Ertl, G. *Science* **1995**, *269*, 668.
(14) Flätgen, G.; Krischer, K. *J. Chem. Phys.* **1995**, *103*, 5428.
(15) Flätgen, G.; Krischer, K. *Phys. Rev. E* **1995**, *51*, 3997.
(16) Flätgen, G.; Krischer, K.; Ertl, G. *Z. Naturforsch.* **1995**, *50a*, 1097.
(17) Christoph, J.; Strasser, P.; Eiswirth, M.; Ertl, G. *Science* **1999**, *284*, 291.
(18) Strasser, P. *Kinetic Oscillations and Spatiotemporal Self-Organization in Electrocatalytic Reactions.* Ph.D. Thesis, Freie Universität Berlin, Berlin, 1999 (http://www.diss.fu-berlin.de/1999/25).
(19) Grauel, P.; Christoph, J.; Flätgen, G.; Krischer, K. *J. Phys. Chem.* **1998**, *102*, 10264.
(20) Grauel, P. *Das Ag/Peroxodisulfat-System*: *Grenzfläche und Raumzeitliche Dynamik.* Ph.D. Thesis, Freie Universität, Fachbereich für Chemie, Berlin, 1999.
(21) Koper, M. T. M.; Sluyters, J. H. *J. Electroanal. Chem.* **1994**, *371*, 149.
(22) Koper, M. T. M. *J. Electroanal. Chem.* **1996**, *409*, 175.
(23) Strasser, P.; Eiswirth, M.; Ertl, G. *J. Chem. Phys.* **1997**, *107*, 991.
(24) Mazouz, N.; Flaetgen, G.; Krischer, K. *Phys. Rev. E* **1997**, *55*, 2260.
(25) Christoph, J.; Otterstedt, R.; Eiswirth, M.; Jaeger, N.; Hudson, J. *J. Chem. Phys.* **1999**, *110*, 8614.
(26) Christoph, J. *Musterbildung auf Elektrodenoberflächen−Theorie von Reaktions−Migrations−Systemen.* Ph.D. Thesis, Freie Universität Berlin, Berlin, 1999.
(27) Strasser, P.; Lübke, M.; Raspel, F.; Eiswirth, M.; Ertl, G. *J. Chem. Phys.* **1997**, *107*, 979.
(28) Turing, A. *Philos. Trans. R. Soc. London, Ser. B.* **1952**, *327*, 37.
(29) Zhabotinski, A.; Dolnik, M.; Epstein, I. *J. Chem. Phys.* **1995**, *103*, 10306.
(30) Strasser, P.; Lübke, M.; Eickes, C.; Eiswirth, M. *J. Electroanal. Chem.* **1999**, *462*, 19.
(31) Murray, J. *J. Theor. Biol.* **1982**, *98*, 143.
(32) Murray, J. *Mathematical Biology*; Springer-Verlag: New York, 1989.
(33) Castets, V.; Dulos, E.; Boissonade, J.; Kepper, P. D. *Phys. Rev. Lett.* **1990**, *64*, 2953.
(34) Ouyang, Q.; Swinney, H. *Nature* **1991**, *352*, 610.
(35) Vigil, R. D.; Ouyang, Q.; Swinney, H. *Phys. A* **1992**, *188*, 17.
(36) Wit, A. D.; Dewel, G.; Brockmans, P. *Phys. Rev. E* **1993**, *48*, R4191.
(37) Watzl, M.; Münster, A. *Chem. Phys. Lett.* **1995**, *242*, 273.
(38) Stössel, R.; Münster, A. *Chem. Phys. Lett.* **1995**, *239*, 354.
(39) Dolnik, M.; Zhabotinsky, A.; Epstein, I. *J. Phys. Chem.* **1996**, *100*, 6604.
(40) Krömker, S. Wave Bifurcation. In *Proceedings of the 3rd Workshop on Modelling of Chemical Reaction Systems*; Behrendt, F., Warnatz, J., Eds.; IWR: Heidelberg, 1997.
(41) Jakubith, S.; Rotermund, H.; Engel, W.; Oertzen, A. V.; Ertl, G. *Phys. Rev. Lett.* **1990**, *65*, 3013.
(42) Eiswirth, M.; Bär, M.; Rotermund, H. *Phys. D* **1995**, *84*, 40.
(43) Zhukov, S.; Barelko, V. *Sov. J. Chem. Phys.* **1982**, *4*, 883.
(44) Volodin, Y.; Barelko, V.; Merzhanov, A. *Sov. J. Chem. Phys.* **1982**, *5*, 1146.
(45) Philippou, G.; Luss, D. *Chem. Eng. Sci.* **1993**, *48*, 2313.
(46) Luss, D. *Phys. A* **1992**, *188*, 68.
(47) Middya, U.; Sheintuch, M.; Graham, M.; Luss, D. *Phys. D* **1993**, *63*, 393.
(48) Middya, U.; Graham, M.; Luss, D.; Sheintuch, M. *J. Chem. Phys.* **1993**, *98*, 2823.
(49) Krömker, S. *Model and Analysis of Heterogeneous Catalysis with Phase Transitions.* Ph.D. Thesis, University Heidelberg, Heidelberg, 1997.
(50) Otterstedt, R.; Plath, P.; Jaeger, N.; Hudson, J. *J. Chem. Soc. Faraday Trans.* **1996**, *92*, 2933.
(51) Raspel, F.; Eiswirth, M. *J. Phys. Chem.* **1994**, *98*, 7613.
(52) Raspel, F. *Zur Mechanistischen Grundlage Elektrochemischer Oszillatoren*: *Die Oxidation Von Ameisensäure und Wasserstoff an Platinelektroden*, Ph.D. Thesis, Freie Universität Berlin, Berlin, 1996.